Supporting Informations: Quantum Nature of Light in Non-Stoichiometric Bulk Perovskites

Daniel G. Suárez-Forero,[†,‡] Antonella Giuri,[†,‡] Milena De Giorgi,[*,†] Laura Polimeno,[†,¶] Luisa De Marco,[†] Francesco Todisco,[†] Giuseppe Gigli,[†,¶] Lorenzo Dominici,[†] Dario Ballarini,[†] Vincenzo Ardizzone,[†,¶] Benny D. Belviso,[§] Davide Altamura,[§] Cinzia Giannini,[§] Rosaria Brescia,[‖] Silvia Colella,[†,¶] Andrea Listorti,[*,†,¶] Carola Esposito Corcione,[†,‡] Aurora Rizzo,[†,¶] and Daniele Sanvitto[†,⊥]

†*CNR NANOTEC, Institute of Nanotechnology, Via Monteroni, 73100 Lecce, Italy*

‡*Dipartimento di Ingegneria dell'Innovazione, Università del Salento, via per Monteroni, km 1, 73100 Lecce, Italy'*

¶*Dipartimento di Fisica, Universitá del Salento, Strada Provinciale Lecce-Monteroni, Campus Ecotekne, Lecce 73100, Italy*

§*Istituto di Cristallografia, CNR-IC, Via Amendola 122/O, 70126 Bari, Italy*

‖*Electron Microscopy Facility, Istituto Italiano di Tecnologia, via Morego 30, Genova, Italy*

⊥*INFN Sezione di Lecce, 73100 Lecce, Italy*

E-mail: milena.degiorgi@nanotec.cnr.it; andrea.listorti@gmail.com

Optimization of growth process

Formamidinium lead iodide perovskite (FAPI) polycristalline films have been prepared optimizing the growth process. The influence on the optical properties of stoichiometry, annealing temperature and spin speed of film preparation have been studied. Fig. S1 shows the PL spectra of two samples with different stoichiometries annealed at 170°C. Whereas the FAPI 1:1 sample (Fig. 1b) has a rather uniform gaussian spectrum (Fig. S1a), in the FAPI 2:1 sample the presence of narrow peaks can be noticed in rather complex structures.

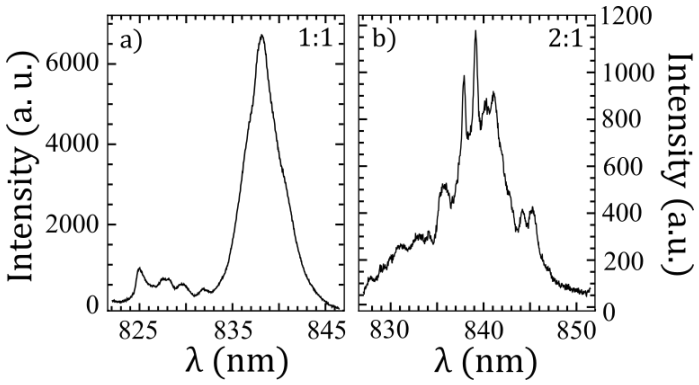

Figure S1: PL spectra of samples annealed at 170°C with stoichiometry 1:1 (left) and 2:1 (right). In both cases the emission is broad, which indicates that additional thermal energy provided during the annealing could induce coalescence of small domains, and therefore, the formation of bigger not confined clusters.

However, none of them is spectrally isolated. By lowering the annealing temperature at 100°C, the spectrum of the non stoichiometric sample shows the presence of very narrow and isolated peaks (Fig. S2a) characterized by a second order correlation function $g^{(2)} < 0.5$. This is an indication that additional thermal energy provided during the annealing could induce coalescence of small domains, and therefore, the formation of bigger not confined clusters respect the ones found by HRTEM measurements and reported in the Fig. 1 of the main text.

To elucidate better the effects of the stoichiometry, we also analyzed samples with different formamidinium-lead iodide ratio: 1.5:1, 2:1, and 3:1 annealed at 100°C. In the FAPI 1.5:1 sample (Fig. S3a), the spectrum becomes more structured compared to the stochiomet-

ric sample, with the appearance of some narrow peaks inside a strong background emission. Further increasing the stochiometric ratio, it was possible to find very narrow and more isolated peaks (Fig. S3b-c). Moreover, the superficial density of emitters and noise-to-signal ratio change considerably as the stoichiometric ratio is increased (Fig. S3d-f). The number of emitting centers decreases, rendering difficult to find isolated narrow peaks on the samples with stoichiometries 3:1. Finally, by increasing the spin coating speed (from 7000 rpm to 12000 rpm), we are able to reduce the thickness of the film resulting in a lower background contribution, as shown in the Fig. S4 obtained on the non-stochiometric FAPI 2:1 annealed at 100°C. The photoluminescence analysis performed on all the samples realized with different growth parameters suggested that the best 0-D confined domains are observed in the sample FAPI 2:1 annealed at 100°C.

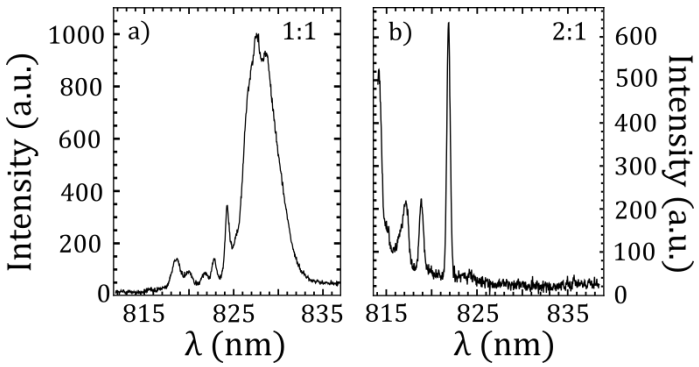

Figure S2: PL spectra of samples annealed at 100°C with different stoichiometries: a) 1:1, b) 2:1. In the stoichiometric case (a) very few emissive regions were found, and those analyzed present broad (yet structured) spectra. In the other case narrow peaks were found.

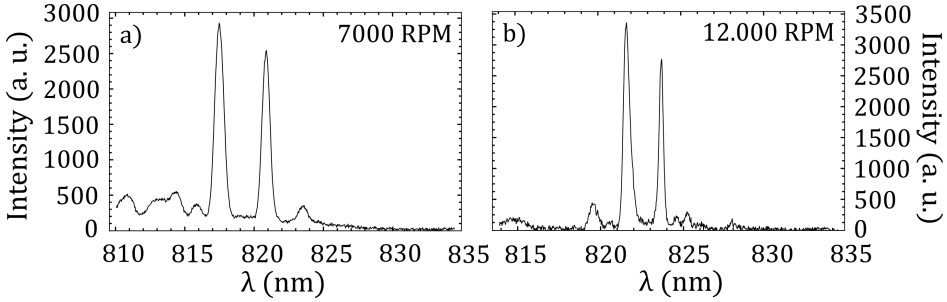

Figure S4: PL spectra of non stochiometric FAPI 2:1 samples annealed at 100°C and obtained with a spin speed of 7000(a) and 12000(b) rpm, respectively.

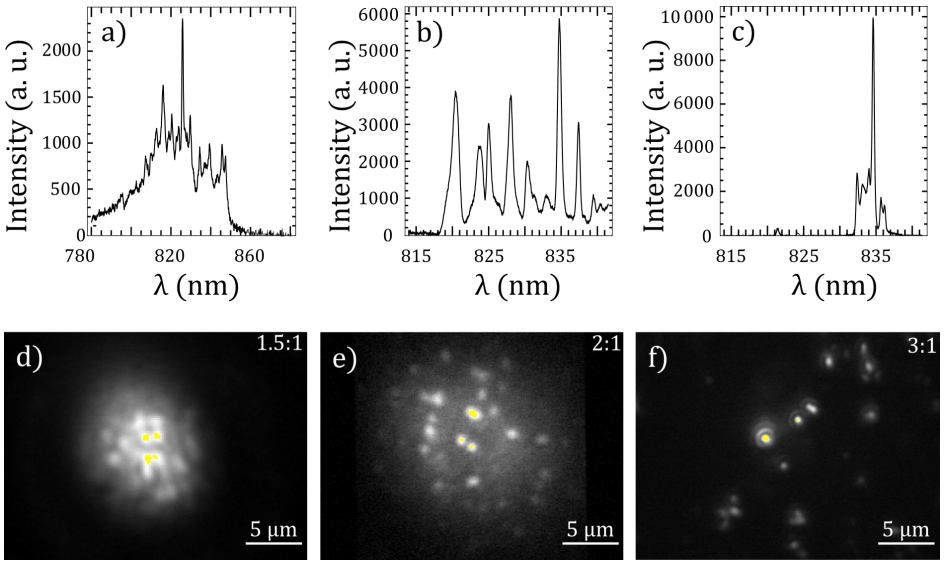

Figure S3: PL spectra and real space emission images of samples annealed at 100°C with stoichiometry 1.5:1 (a-d), 2:1 (b-e) and 3:1 (c-f), respectively, obtained by pumping the samples with a wide spot (diameter around 20 μm) of a 420 nm pulsed laser. Images are taken at T = 4 K.

TEM characterization

High-resolution transmission electron microscopy (HRTEM) investigations and energy-dispersive X-ray spectroscopy (EDS) analyses were performed on perovskite thin films spin-coated onto carbon-coated Cu grids for TEM (spin-coating on C film side). Figure S5 shows a region of FAPI 1:1 polycrystalline film in which δ phase is detectable.

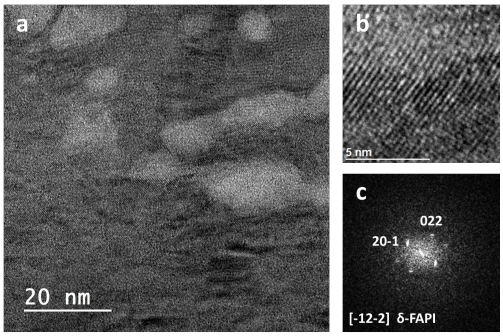

Figure S5: (a) HRTEM image of the film FAPI 1:1 and (b) a portion of it. (c) FFT of (b), matching with δ-FAPI.

FAPI 1:1			
Element	Netto	Atom [%]	rel. Error [%] (1 sigma)
Iodine	22045	54.76	10.08
Nitrogen	708	26.77	5.55
Lead	7792	18.46	10.19
	Sum	100	
I (at. %) / N (at. %) / Pb (at. %) = 3.0 : 1.4 : 1			

FAPI 2:1			
Element	Netto	Atom [%]	rel. Error [%] (1 sigma)
Iodine	28621	52.60	10.07
Nitrogen	1195	33.45	4.70
Lead	7956	13.95	10.20
	Sum	100	
I (at. %) / N (at. %) / Pb (at. %) = 3.8 : 2.4 : 1			

Figure S6: Composition of the two samples evaluated by STEM-EDS analyses which revealed a higher amount of nitrogen (from formamidinium) and iodine with respect to the lead amount in 2:1 perovskite.

XRD and XRF Experiments

XRD patterns were collected in coupled sample-detector scan mode ($\theta/2\theta$), with 0.05° (2θ) step size. A Bruker D8 Discover diffractometer was employed, equipped with a Göbel mirror using CuKα radiation ($\lambda = 1.54$ $\mathring{A}$) and a scintillation detector.

Qualitative phase analysis was performed by using QualX,[?] returning the - (trigonal) and - (hexagonal) formamidinium lead iodide crystalline phases (corresponding thttps://es.overleaf.com/1489923 data_4335631 and data_4335640, respectively, of the Crystallography Open Database, COD [http://www.crystallography.net]). In the Fig. S7, the expected powder XRD patterns for the two crystalline phases are reported, below the experimental ones,showing the coexistence of both phases in the FAPI 1:1 sample, and the presence of the only α-phase in the FAPI 2:1 sample. Moreover, the comparison between the relative peak intensities indicates a 100 preferred orientation for the δ-phase and a 101 preferred orientation for the α-phase. Scanning combined XRF/XRD experiments, with a 28 μm (diameter) beam, were performed on the XRD1 synchrotron beamline at ELETTRA to obtain at the same time information about the relative amount of iodide and lead, as well as structural features, in a large area of the two samples. Principal Component Analysis (PCA) of the regions around I-L3M5 and Pb-L3M5 (between 3.3 and 4.7 and between 9.8 and 11.2 KeV for iodide and lead, respectively), which represent the peaks having higher fluorescence yield in the analysed energy range, was performed to group rescaled data. This procedure allowed to group data with

similar I-L3M5/Pb-L3M5 ratios in clusters. The most representative cluster of each sample and its fitting is shown in Fig. S8. In addition to iodide and lead, spectra show the presence of iron, cobalt, nickel, and copper coming from the substrate. The resulting ratio between the I-L3M5 and Pb-L3M5 signal areas is reported in Fig. S9. It can be recognized from Fig S8 that PCA results in 2 clusters for both the samples, one of which contains very few profiles (one and two for FAPI 1:1 and FAPI 2:1, respectively). This suggests high sample homogeneity within the scanned area, as confirmed by the low variance explained by the first principal component (<10%) in both samples. Fig. S9 shows the ratio between L3M5 transitions of I and Pb. This ratio clearly indicates statistically significant differences of the I/Pb relative amount between the two samples. The I/Pb ratio is smaller by approximately 20% in FAPI 1:1 with respect to FAPI 2:1, in agreement with the trend expected based on the precursor different ratios.

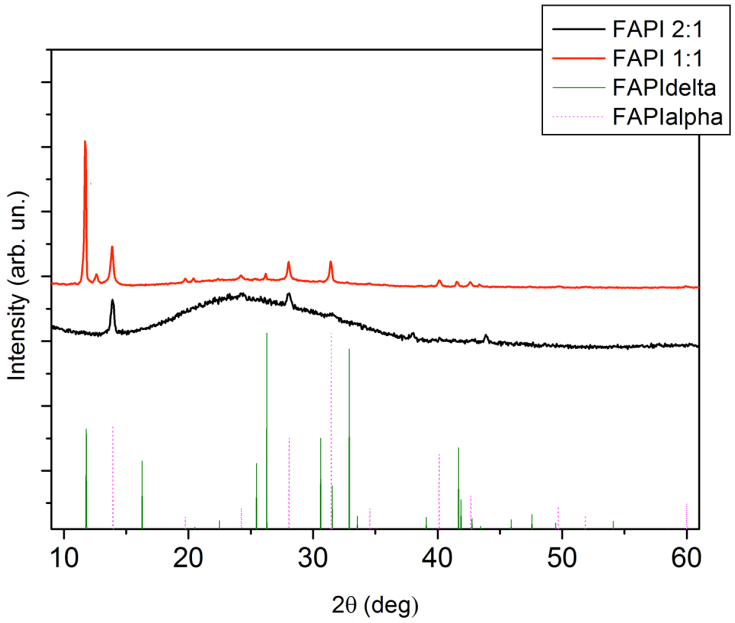

Figure S7: XRD patterns of stoichiometric (solid red line) and non stoichiometric (solid black line) FAPI. Vertical lines indicate the originating phase of every peak in the pattern: dashed pink lines are for α phase and solid green lines are for δ phase. Samples with balanced quantities of organic and inorganic components present a coexistence of α and δ phase, while in samples with excess of FAI only α phase is detected.

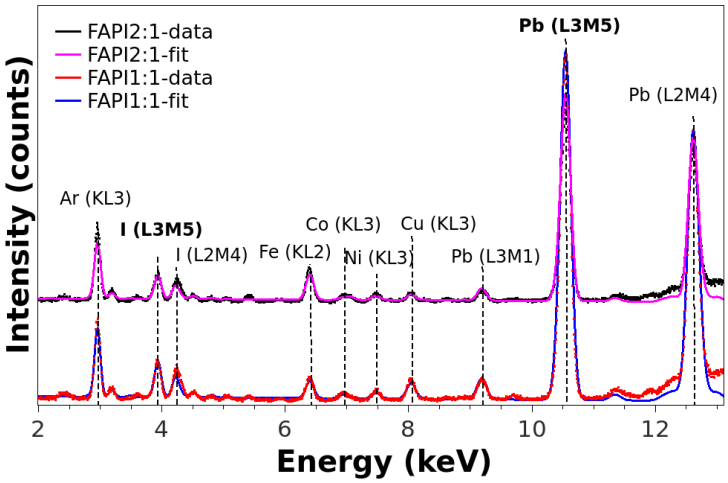

Figure S8: X-ray fluorescence data (black and red points for FAPI 2:1 and 1:1, respectively) and fit results (magenta and blue lines for FAPI 2:1 and 1:1, respectively) related to averaged fluorescence spectra of the most representative cluster for both samples. The curves have been vertically shifted for clarity sake. Position for each peak detected in our samples has been pointed out by a dotted line. I-L3M5 and Pb-L3M5 peaks used in the analysis of Fig. S5 are labelled in bold.

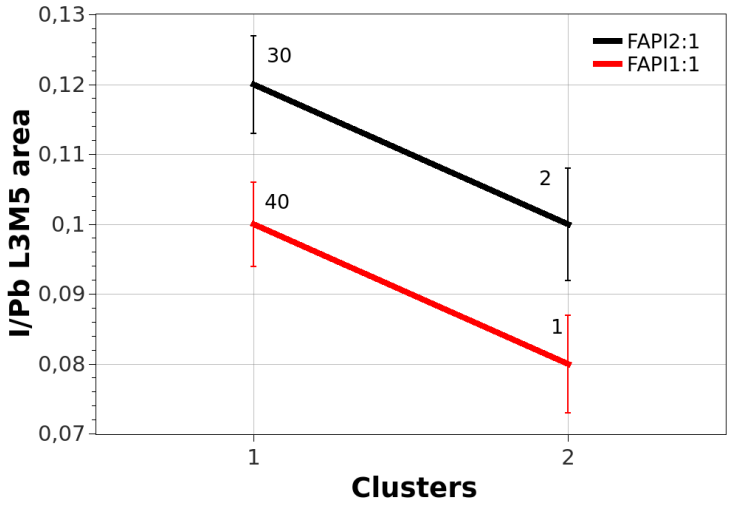

Figure S9: Ratio between the areas of the L3M5 transition of iodide and lead for FAPI 2:1 and 1:1 (black and red line, respectively). The error bar for each ratio is the absolute error resulting from the fitting procedure. The number of averaged spectra for each cluster is reported as a label.

Time dependent PL experiments

Time dependent PL spectral measurements were performed by measuring the single quantum dots spectra at different time intervals in a range between 1 and 90 m. In particular, Fig. S10 shows that also at longer times very low spectral diffusion occurs and the FWHM is almost constant which means that no degradation of the material was detected during the first 90 minutes.

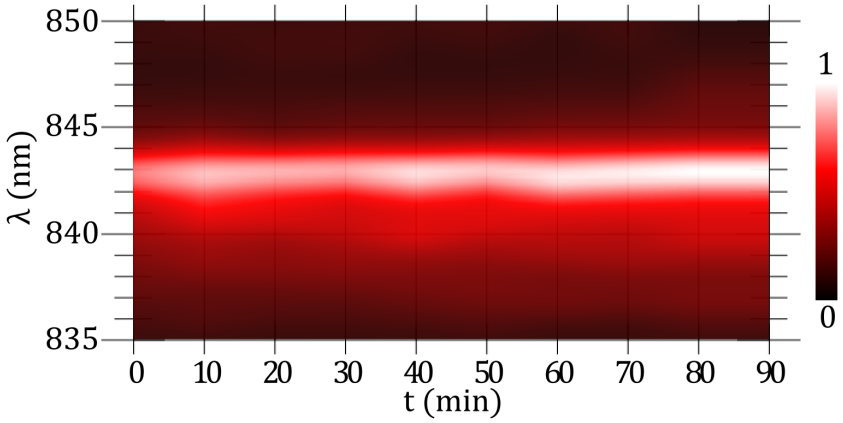

Figure S10: Left: Time dependent PL spectra for long times for a typical QD excited at a power of $1\mu W/\mu m^2$. No degradation of the material was observed in the measured period of 90 minutes.

Statistics of the second order correlation function

$g^{(2)}$ measurements were performed in dots of four samples, grown under similar conditions (FAPI 2:1), to test the statistics and reproducibility of the process. In every case, a narrow peak was spatially and spectrally selected and analyzed with a HBT setup. In general, emissive centers that present isolated peaks in the PL, show antibunching which is an evidence of the quantum nature of the emitters. It is worth nothing that the QD peaks disappear at temperature higher than T = 20 K resulting in a very low exciton ionization energy (E(20K)= kT = 1,7 meV). Accordingly, the energy position of the peaks is very close to the perovskite bulk emission which means that the carrier localization is not very deep. As a

result, the wide emission from the bulk attempts against the purity of the single photons, as it can be seen in Fig. S11. This explains the residual photon coincidences of the $g^{(2)}(0)$. In fact as shown in Fig.S11, the emission in the left panel has a narrow and isolated peak, while in the right panel the bulk emission has a tail that partially overlaps with the wavelength of the dot. This is reflected in the increase of the $g^{(2)}(0)$ from 0.22 ± 0.02 to 0.54 ± 0.05. In every case the integration time varies from one to ten hours.

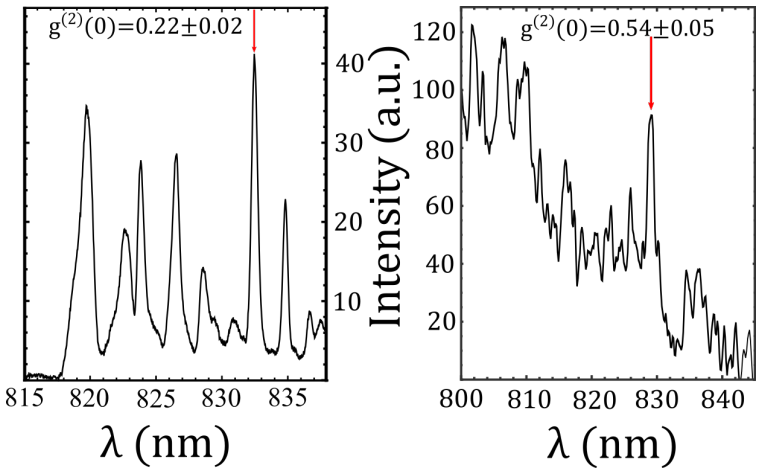

Figure S11: Spectra of two representative quantum dots on sample FAPI 2:1. Notice that while the one with lower value of $g^{(2)}(0)$ (left) shows an isolated peak, the other one, with value greater than 0.5 (right), has the exciton peak overlapped with the bulk emission. Red arrows indicate the peaks on which $g^{(2)}$ measurements were performed after spectral selection.

Radiative decay time

A necessary condition for a single photons source to be genuinely "on-demand", is a low decay time respect to the temporal delay between consecutive pulses. Fig. S12 shows the measured radiative decay time and second order correlation function of representative quantum dots pumped at 780 nm (left) and 420 nm (right). The higher pump energy implies more non-radiative decays, and therefore, greater decay times. Despite this difference in the decay

time, in both cases it is small compared with the temporal delay between successive laser pulses.

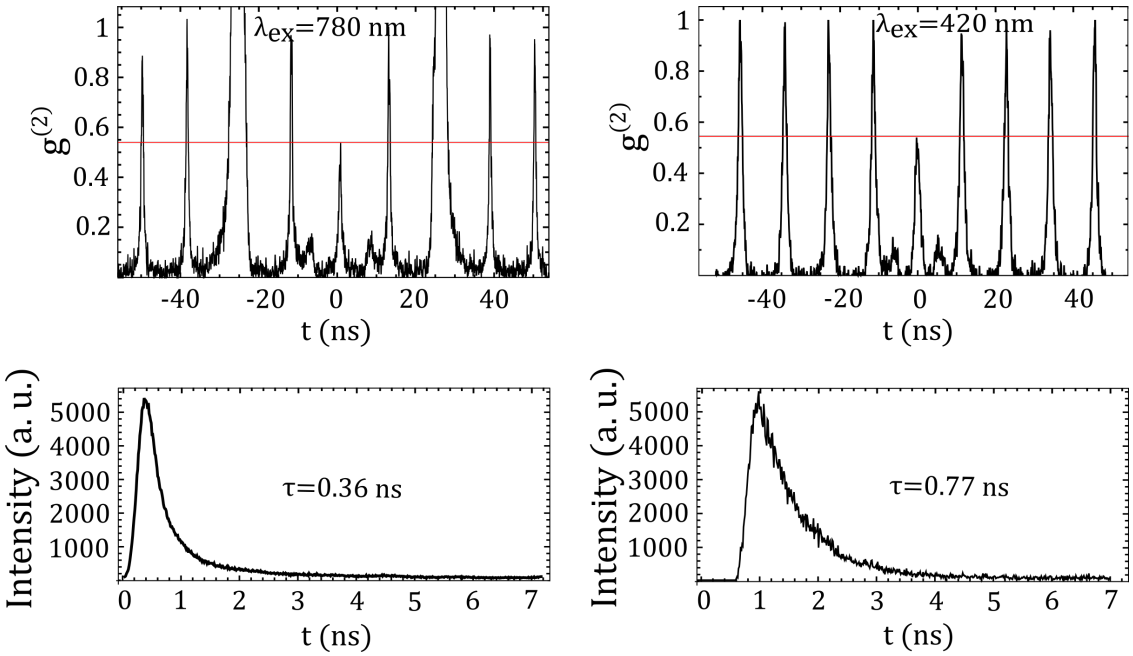

Figure S12: Left: second order correlation function (upper panel) and decay time (lower panel) of a representative quantum dot pumped at 780 nm. Right: second order correlation function (upper panel) and decay time (lower panel) of a representative quantum dot pumped at 420 nm. Although the antibunching is preserved, the decay time increases with the pump energy.